Please cite this article in press as: Zhang et al., Inner Envelope CHLOROPLAST MANGANESE TRANSPORTER 1 Supports Manganese Homeostasis and Phototrophic Growth in *Arabidopsis*, Molecular Plant (2018), https://doi.org/10.1016/j.molp.2018.04.007

Molecular Plant
Research Article

CellPress
PARTNER JOURNAL

Inner Envelope CHLOROPLAST MANGANESE TRANSPORTER 1 Supports Manganese Homeostasis and Phototrophic Growth in *Arabidopsis*

Bin Zhang[1,2,5], Chi Zhang[1,2,5], Congge Liu[1], Yanping Jing[1], Yuan Wang[1], Ling Jin[1], Lei Yang[1], Aigen Fu[2], Jisen Shi[3], Fugeng Zhao[1], Wenzhi Lan[1,*] and Sheng Luan[4,*]

[1]Nanjing University-Nanjing Forestry University Joint Institute for Plant Molecular Biology, College of Life Sciences, Nanjing University, Nanjing 210093, China

[2]The Key Laboratory of Western Resources Biology and Biological Technology, College of Life Sciences, Northwest University, Xi'an, China

[3]Nanjing University-Nanjing Forestry University Joint Institute for Plant Molecular Biology, Key Laboratory of Forest Genetics and Biotechnology, Nanjing Forestry University, Nanjing 210037, China

[4]Department of Plant and Microbial Biology, University of California, Berkeley, CA 94720, USA

[5]These authors contributed equally to this article.

***Correspondence: Wenzhi Lan (lanw@nju.edu.cn), Sheng Luan (sluan@berkeley.edu)**

https://doi.org/10.1016/j.molp.2018.04.007

ABSTRACT

Manganese (Mn) is an essential catalytic metal in the Mn-cluster that oxidizes water to produce oxygen during photosynthesis. However, the transport protein(s) responsible for Mn^{2+} import into the chloroplast remains unknown. Here, we report the characterization of *Arabidopsis* CMT1 (Chloroplast Manganese Transporter 1), an evolutionarily conserved protein in the Uncharacterized Protein Family 0016 (UPF0016), that is required for manganese accumulation into the chloroplast. *CMT1* is expressed primarily in green tissues, and its encoded product is localized in the inner envelope membrane of the chloroplast. Disruption of *CMT1* in the T-DNA insertional mutant *cmt1-1* resulted in stunted plant growth, defective thylakoid stacking, and severe reduction of photosystem II complexes and photosynthetic activity. Consistent with reduced oxygen evolution capacity, the mutant chloroplasts contained less manganese than the wild-type ones. In support of its function as a Mn transporter, CMT1 protein supported the growth and enabled Mn^{2+} accumulation in the yeast cells of Mn^{2+}-uptake deficient mutant (*Δsmf1*). Taken together, our results indicate that CMT1 functions as an inner envelope Mn transporter responsible for chloroplast Mn^{2+} uptake.

Key words: chloroplast inner envelope, manganese transporter, metal transport, oxygen-evolving complex

Zhang B., Zhang C., Liu C., Jing Y., Wang Y., Jin L., Yang L., Fu A., Shi J., Zhao F., Lan W., and Luan S. (2018). Inner Envelope CHLOROPLAST MANGANESE TRANSPORTER 1 Supports Manganese Homeostasis and Phototrophic Growth in *Arabidopsis*. Mol. Plant. ■ ■, 1–12.

INTRODUCTION

Chloroplast houses photosynthesis, the process by which light energy is converted to chemical energy. Photosynthetic light reaction is made possible by two photosystems (photosystem II [PSII] and photosystem I [PSI]) acting sequentially. PSII catalyzes the light-dependent oxidation of water to produce oxygen (Ferreira et al., 2004; Shen, 2015). This reaction, with an additional input of energy from PSI, provides a primary source of reducing equivalents and ATP, which are used to convert carbon dioxide to starch (Shen, 2015).

The native form of PSII resides in the thylakoid membrane, and its core complex is composed of the subunits D1 and D2, which bind the chlorophyll P680 and the α and β subunits of cytochrome b_{559}, CP43 and CP47, and other proteins whose functions are less well characterized (Shen, 2015). The D1 protein is synthesized as a precursor (pD1) with a short C-terminal extension. A thylakoid-localized C-terminal peptidase removes the C-terminal extension to produce the functional mature D1 protein (Che et al., 2013). D1 coordinates with CP43 to form ligands for the Mn_4CaO_5 cluster, the catalytic center of the oxygen-evolving complex (OEC) (Ferreira et al., 2004; Roose and Pakrasi, 2004). In plants, the Mn_4CaO_5 cluster is localized

Published by the Molecular Plant Shanghai Editorial Office in association with Cell Press, an imprint of Elsevier Inc., on behalf of CSPB and IPPE, SIBS, CAS.

Please cite this article in press as: Zhang et al., Inner Envelope CHLOROPLAST MANGANESE TRANSPORTER 1 Supports Manganese Homeostasis and Phototrophic Growth in *Arabidopsis*, Molecular Plant (2018), https://doi.org/10.1016/j.molp.2018.04.007

at the thylakoid lumenal side and is stabilized by at least three lumen-exposed extrinsic proteins (PsbO, PsbP, and PsbQ). As the catalytic center for water splitting, the Mn_4CaO_5 cluster splits two water molecules into four protons and one oxygen molecule, with four electrons to initiate the photosynthetic electron transport through the Z chain (Nelson and Yocum, 2006; Shen, 2015).

In addition to Mn and Ca required for the formation of the water-splitting Mn cluster, a number of other metal ions are also found to be important in chloroplast, such as copper serving as the redox cofactor of plastocyanin and iron as a cofactor in several Fe-containing proteins, including cytochrome and Fe-S proteins (Theg and Wollman, 2014; Pottosin and Shabala, 2016). Metal ions also participate in processes beyond photosynthesis, such as biosynthesis of amino acid (Zn), detoxification of reactive oxygen species (Cu, Zn, and Fe), and other functions (Nouet et al., 2011; Pottosin and Shabala, 2016). Despite important functions of metal ions in the chloroplast, the molecular mechanism underlying ion transport across chloroplast membranes remains a poorly understood subject. Chloroplasts are double membrane-bound organelles enclosed by an outer and an inner envelope membrane. While the outer envelope membrane is permeable to most ions (Finazzi et al., 2014; Oh and Hwang, 2015), the inner membrane should be equipped with a unique set of transmembrane proteins that transport metal ions into and out of chloroplasts (Finazzi et al., 2014; Carraretto et al., 2016; Pottosin and Shabala, 2016). In addition, some of the metal ions must be transported further into the thylakoid lumen through the transporters localized in the thylakoid membrane. While PAA1 and PAA2 have been shown to transport Cu into the chloroplast stroma and further into the thylakoid lumen (Shikanai et al., 2003; Abdel-Ghany et al., 2005), the molecular mechanisms underlying transport of most other metal ions remain less understood. Concerning Mn/Ca-transport proteins, a recent study has identified a thylakoid-localized transmembrane protein, PHOTOSYNTHESIS AFFECTED MUTANT71 (PAM71), as critical for the biogenesis of Mn_4CaO_5 cluster (Schneider et al., 2016). This protein is also referred to as chloroplast-localized Ca^{2+}/H^+ antiporter 1 (CCHA1) in an independent report, suggesting a function in chloroplast Ca^{2+} and pH homeostasis (Wang et al., 2016).

To identify chloroplast metal transporters, we screened *Arabidopsis* mutant lines containing transfer DNA (T-DNA) insertions in genes encoding "uncharacterized transmembrane proteins" and scored those with phenotypic defects in photosynthesis. In this study, we identified a gene *CMT1* (*Chloroplast Manganese Transporter 1*) (*AT4G13590*) encoding a transporter belonging to the highly conserved UPF0016 (Uncharacterized Protein Family 0016) family and showed that it is required for PSII function, chloroplast development, and plant growth. We found that CMT1 is localized in the inner envelope membrane and is essential for Mn^{2+} homeostasis in chloroplasts.

RESULTS

Identification of a Mutant with Defective Autotrophic Growth

A large portion of the *Arabidopsis* genome encodes functionally unknown proteins with multiple transmembrane domains. Many of these proteins may function as transporters of various substrates. We screened the T-DNA insertion mutants of these genes and scored those with obvious phenotypic defects. We found that seedlings of a mutant line (stock number SALK_129037) appeared stunted and yellowish when grown on half-strength Murashige and Skoog (MS) medium containing 1% sucrose (Supplemental Figure 1A). We confirmed by genomic PCR that the yellow seedlings were homozygous individuals that contained a T-DNA insertion in the gene *AT4G13590* (Supplemental Figure 1B). We then planted the seeds produced by the homozygous and heterozygous plants and found that all F2 progeny of the former were yellowish and stunted, lacking *AT4G13590* transcript, and F2 progeny of the latter segregated normal and defective seedlings with the ratio of 3:1 (Supplemental Table 1). These results suggest that the phenotype was caused by the disruption of a single gene. We named the gene *AT4G13590* as *Chloroplast Manganese Transporter 1* (*CMT1*) and the mutant line (SALK_129037) containing a T-DNA insertion in the second intron of this gene (Figure 1A) as *cmt1-1* based on our research described in this article.

To verify that the aberrant growth of *cmt1-1* is specific for the disruption of *CMT1*, a second mutant allele (SALK_011783) with a T-DNA insertion in the 5′-UTR of *CMT1* (Figure 1A), referred to as *cmt1-2,* was also included. RT–PCR analysis showed that *cmt1-1* lacked a detectable level of *CMT1* transcript, whereas *cmt1-2* still expressed *CMT1* mRNA albeit at a reduced level compared with the wild-type (Figure 1B). Thus, *cmt1-1* and *cmt1-2* were knockout and knockdown mutants, respectively. Unlike the *cmt1-1* mutant that showed a distinctive growth phenotype with a severely stunted yellowish rosette (Figure 1C and Supplemental Figure 2A–2C), *cmt1-2* plants were similar to the wild-type, suggesting that the reduced level of *CMT1* expression in the knockdown mutant did not alter the normal growth of *Arabidopsis* (Figure 1C–1E). When plants were cultivated in the soil, the *cmt1-1 plants* exhibited a severely dwarf phenotype with small yellowish leaves and low yield compared with the wild-type (Supplemental Figure 2D). To confirm that the phenotype was caused by the mutation of *CMT1*, a 4552 bp genomic DNA of *CMT1* including the promoter, coding region, and 3′-UTR was transformed into *cmt1-1* for the complementation test. We found that this fragment fully complemented the *cmt1-1* phenotype back to the wild-type (Figure 1B–1E), supporting the conclusion that disruption of the *CMT1* gene caused the growth defects in the *cmt1-1* mutant plants.

To examine the expression pattern of the *CMT1* gene in *Arabidopsis* plants, we performed quantitative real-time PCR (qRT–PCR) assay and found that *CMT1* mRNA was high in the leaves, stems, flowers, and siliques, but low in the roots (Figure 1F). To assess the expression pattern of *CMT1* in further detail, we analyzed the transgenic plants expressing the β-glucuronidase (GUS) reporter driven by a 1975 bp promoter fragment of *CMT1*. GUS staining analysis revealed that *CMT1* was strongly expressed in the leaves and other green parts of the plant such as stems, flower organs, and siliques (Figure 1G), which was consistent with the qRT–PCR analysis.

Please cite this article in press as: Zhang et al., Inner Envelope CHLOROPLAST MANGANESE TRANSPORTER 1 Supports Manganese Homeostasis and Phototrophic Growth in *Arabidopsis*, Molecular Plant (2018), https://doi.org/10.1016/j.molp.2018.04.007

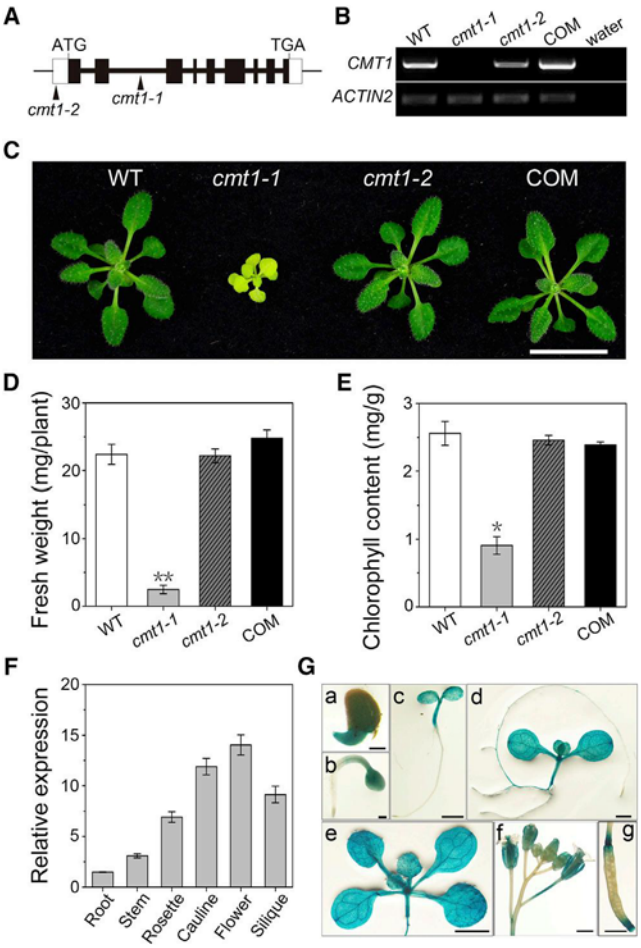

Figure 1. Genetic Characterization of *cmt1* Mutant Plants.

(A) *Arabidopsis CMT1* gene structure and localization of the T-DNA insertion sites in *cmt1-1* and *cmt1-2* lines. The *CMT1* gene contains nine exons (black boxes) and eight introns (bold black lines). The 5′- and 3′-UTRs are indicated by open boxes. ATG, translation start codon; TGA, stop codon.

(B) RT–PCR analysis of wild-type (WT), *cmt1-1*, *cmt1-2*, and *cmt1-1* transformed with *CMT1* genomic DNA (COM). *ACTIN2* was used as a loading control. Water was used as a negative control.

(C) Phenotype of WT, *cmt1-1*, *cmt1-2*, and COM plants grown on half-strength Murashige and Skoog (MS) medium with 1% sucrose (w/v) for 3 weeks under growth light (90 μmol/m^2/s) with a long-day cycle (16 h light/8 h dark). Scale bar, 1 cm.

(D and E) (D) Fresh weight and **(E)** chlorophyll content of 3-week-old plants shown in **(C)**. Data are means ± SD. n = 4 for each genotype. Asterisks indicate statistically significant differences compared with WT (Mann-Whitney test, **P* < 0.05 and ***P* < 0.01).

(F) Relative expression level of *CMT1* in different tissues (root, stem, rosette leaf, cauline leaf, flower. and silique) of 5-week-old WT plants grown in hydroponic culture medium. The expression level was determined by quantitative real-time RT–PCR. *ACTIN2* was used as an internal standard. Data are means ± SD. n = 4.

(G) Expression pattern of $CMT1_{pro}$*::GUS* in transformed *Arabidopsis* plants at different growth stages and tissues **(a)** 1 day, **(b)** 2 days, **(c)** 3 days, **(d)** 7 days, **(e)** 10 days, **(f)** inflorescence. and **(g)** silique. Scale bars: 200 μm in **(a)** and **(b)**; 1 mm in **(c–g)**.

CMT1 Is Localized in the Chloroplast Inner Envelope Membrane

The *CMT1* gene is predicted to encode a transmembrane protein with a cTP (chloroplast Transit Peptide) in its N terminus (Supplemental Figure 3A–3C), and its protein product was previously identified in the proteome extracted from the chloroplast inner envelope preparation (Ferro et al., 2003, 2010). To further assess the subcellular localization of CMT1, a *CMT1-GFP* fusion was cloned into a vector under the control of the constitutive *35S* cauliflower mosaic virus promoter and introduced into *Arabidopsis* mesophyll protoplasts by transient transfection. Confocal laser scanning microscopic analysis indicated that the CMT1-GFP fluorescence signal was specifically associated with the periphery of the chloroplast, in contrast to the control GFP signal present in the cytosol (Figure 2A and 2B). Furthermore, when chloroplasts were released from the mesophyll protoplasts transfected by CMT1-GFP, GFP signals were again detected at the chloroplast periphery (Figure 2G), indicating that CMT1 is localized to the chloroplast.

Chloroplast consists of multiple membrane systems. To find out the accurate localization of CMT1 in the chloroplast, we utilized several chloroplast proteins, including PIC1 for the inner envelope membrane (Duy et al., 2007), OEP7 for the outer envelope membrane (Lee et al., 2001), PAA2 for the thylakoid membrane (Abdel-Ghany et al., 2005), and RBCS for stroma (Lee et al., 2006), to serve as sub-organelle location references. As shown in Figure 2, fluorescence signals from CMT1-GFP decorated the perimeter of the chloroplast in a dotted fashion, similar to distribution of PIC1-GFP, the inner envelope marker. To further confirm the localization of CMT1 in the inner envelope membrane, we co-transfected CMT1-GFP with either PIC1-RFP or OEP7-RFP into mesophyll protoplasts. The confocal images showed that punctate signals of CMT1-GFP co-localized with PIC1-RFP with high correlation co-efficiency (Figure 2I), but not with OEP7-RFP (Figure 2J). Hence, we conclude that CMT1 is localized to the inner envelope membrane of chloroplasts.

CMT1 Is Crucial for Chloroplast Development, Photosynthetic Activity, and Assembly of PSII Complexes

Localization of CMT1 to the chloroplast envelope and the severely stunted and yellowish rosette of *cmt1-1* mutant suggested a function of CMT1 in the chloroplast and photosynthesis. To explore the CMT1 function in more detail, we examined the morphology and the ultrastructure of leaf tissue and chloroplasts in the wild-type and *cmt1-1* mutant. The overall cross-section of the leaf tissue appeared similar in the *cmt1-1* mutant and the wild-type, but the number and size of the starch grains were significantly decreased in *cmt1-1* (Figure 3A–3D and Supplemental Figure 4). Under transmission electron microscopy, chloroplasts in *cmt1-1* displayed fewer stacked grana lamellae than those in the wild-type (Figure 3E–3H). These results indicated that loss of function of CMT1 alters the structure of the thylakoid membrane and thus photosynthetic activity, leading to less starch synthesis.

To access the role of CMT1 in photosynthesis, we initially measured the chlorophyll *a* fluorescence of intact leaves. Compared with the wild-type, the *cmt1-1* mutant showed a

Please cite this article in press as: Zhang et al., Inner Envelope CHLOROPLAST MANGANESE TRANSPORTER 1 Supports Manganese Homeostasis and Phototrophic Growth in *Arabidopsis*, Molecular Plant (2018), https://doi.org/10.1016/j.molp.2018.04.007

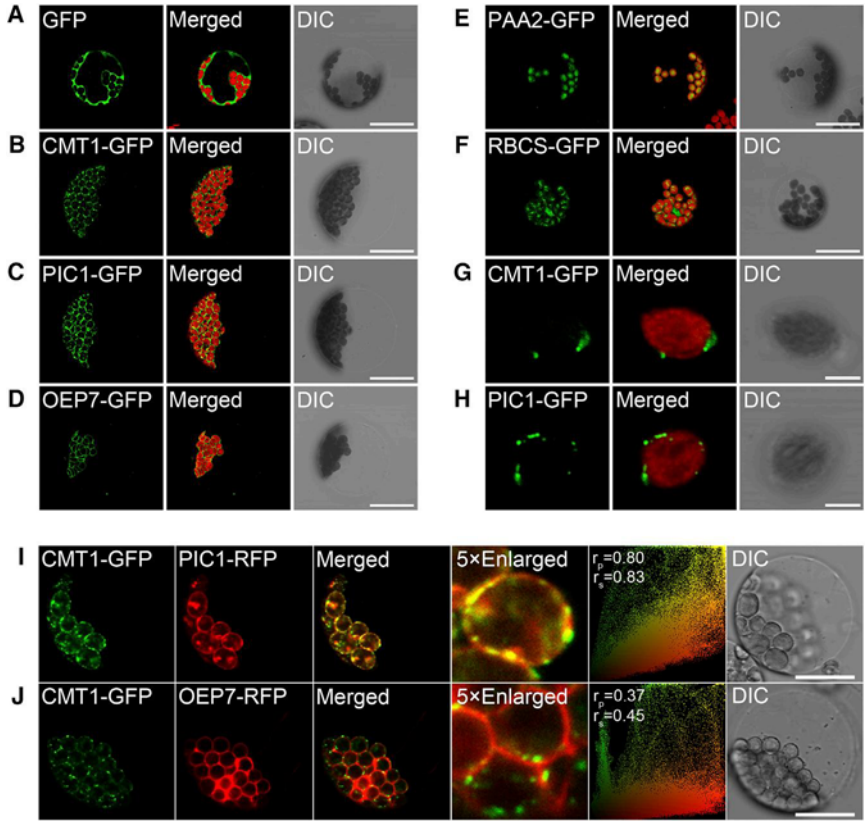

Figure 2. Localization of CMT1 in the Inner Envelope of Chloroplasts.

(A–F) *Arabidopsis* protoplasts were transiently transformed with *GFP* **(A)**, *CMT1-GFP* **(B)**, *PIC1-GFP* **(C)**, *OEP7-GFP* **(D)**, *PAA2-GFP* **(E)**, and *RBCS-GFP* **(F)**. Scale bars, 20 μm.

(G and H) The single chloroplast released from the protoplasts expressing CMT1-GFP **(G)** or PIC1-GFP **(H)**. Scale bars, 5 μm.

(I and J) Columns from left to right show GFP signals, merged images of GFP, and chlorophyll autofluorescence (Merged) and bright-field differential interference contrast (DIC), respectively. CMT1-GFP was co-expressed with PIC1-RFP **(I)** and OEP7-RFP **(J)** fusion proteins in the *Arabidopsis* protoplasts. Columns from left to right show GFP signals, RFP signals, merged images of GFP and RFP (Merged), 5× enlargement of a randomly selected area of merged images (5× Enlarged), and DIC, respectively. Colocalization from columns three is depicted as relative intensity (X and Y axes) scatterplots. Values of r_p and r_s coefficients were calculated and are shown next to the scatterplots. Scale bars, 20 μm.

significant decrease in the maximum quantum yield (F_v/F_m) (Figure 4A) and the effective quantum yield (ΦPSII) (Figure 4B) at different photon flux densities, indicating a functional impairment of PSII. In addition, 1 − qL, reflecting the redox state of the Q_A electron acceptor of PSII, was higher in the *cmt1-1* mutant, implying a defective electron transfer between PSII and Q_A in the mutant (Supplemental Table 2). We also monitored non-photochemical quenching (NPQ) and found it to be higher in the mutant at low light intensities ($\leq$74 μmol/m^2/s), which implied a higher proportion of energy dissipation in the form of heat due to the impairment of PSII and electron transfer (Supplemental Table 2). Another parameter reflecting the activity of PSII is the oxygen evolution rate, which can be measured with isolated thylakoid membranes using potassium ferricyanide as the artificial electron acceptor. In the wild-type thylakoid preparation, the oxygen evolution exhibited a rapid increase when actinic light (AL) was turned on, whereas the *cmt1-1* mutant preparation had severely reduced oxygen production, only up to 32% of the wild-type level (Figure 4C and 4D). Collectively, these results indicated that the CMT1 is crucial for PSII activity and electron transport, which is consistent with the stunted growth of mutant plants.

The defects in PSII activity were possibly caused by a reduced level or malfunction in protein supercomplexes (SCs) in the electron transport chain. To examine possible changes in the organization of thylakoid protein complexes in the *cmt1-1* mutants, we solubilized the thylakoid membrane samples with β-dodecyl maltoside and analyzed the abundance of various photosynthetic complexes by blue native gel electrophoresis (BN–PAGE). As shown in Figure 5A, the banding pattern of the protein complexes revealed significant differences when comparing the mutant with the wild-type. In particular, the levels of higher-molecular-weight supercomplexes were dramatically reduced in *cmt1-1* mutant (Figure 5A). By contrast, the abundance of LHCII trimer (LHCII-T) and LHCII monomer (LHCII-M) increased in *cmt1-1* (Figure 5A). When BN–PAGE slices were subjected to a second dimensional (2D) SDS–PAGE in combination with silver stain, we observed a dramatic decrease in the abundance of protein subunits associated with the PSII SCs (D1, D2, CP43, and CP47), while protein spots in the area corresponding to the LHCII trimer and monomer were significantly increased in the *cmt1-1* samples (Figure 5B). In addition, the mutant was almost devoid of subunits in cytochrome b_6/f complex (PetB, PetC, and PetD) that were readily detected in the wild-type (Figure 5B).

To assess more quantitatively the changes in the *cmt1-1* mutant, we performed an immunoblotting assay using a set of antibodies against representative subunits of the four major photosynthetic complexes in the thylakoid membrane. The result showed that the levels of PSI subunits (PsaA, PsaD, and PsaF) and the β subunit of ATP synthase (ATPβ) were not altered (Figure 5C). However, PSII core subunits (D1, D2, and CP43), as well as subunits of the cytochrome b_6/f complex (Cyt *f* and PetC) were reduced to about 50% of wild-type levels (Figure 5C). As the major protein components of the OEC, the PsbO level was unchanged in *cmt1-1*, but the abundance of PsbP and PsbQ showed a noticeable reduction compared with the wild-type (Figure 5C). Taking the above results into consideration, the *cmt1-1* mutant is mainly defective in PSII.

CMT1 Plays a Key Role in Chloroplast Mn Homeostasis

CMT1 belongs to UPF0016 family, which is evolutionally conserved in all eukaryotes, many bacteria, and archae (Supplemental

Please cite this article in press as: Zhang et al., Inner Envelope CHLOROPLAST MANGANESE TRANSPORTER 1 Supports Manganese Homeostasis and Phototrophic Growth in *Arabidopsis*, Molecular Plant (2018), https://doi.org/10.1016/j.molp.2018.04.007

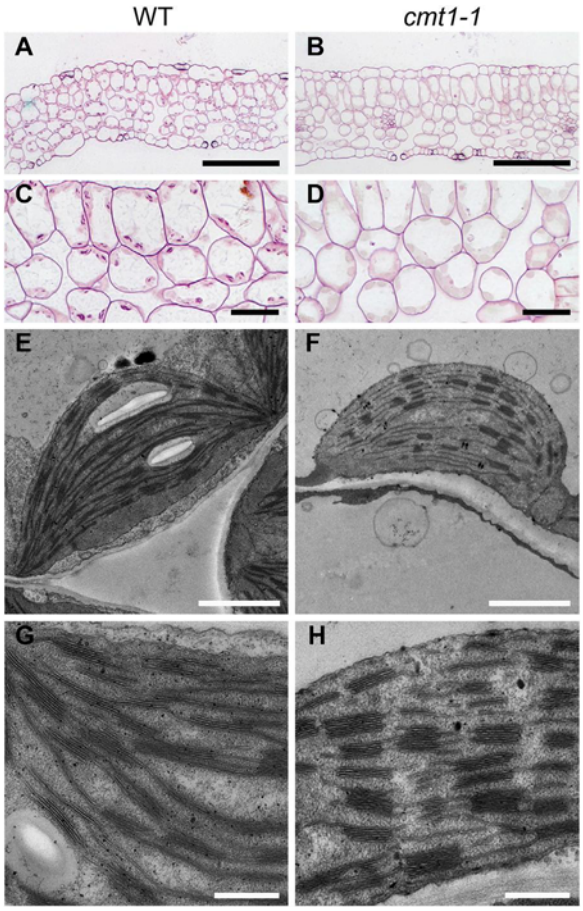

Figure 3. Loss of CMT1 Function Affects Chloroplast Development.

(A–D) Light microscopy of cross-sections of rosette leaves from 3-week-old WT (**A** and **C**) and *cmt1-1* plants **(B and D)**. Scale bars: 50 μm in **(A)** and **(B)**; 10 μm in **(C)** and **(D)**.

(E–H) Transmission electron microscopy of chloroplasts from 3-week-old WT (**E** and **G**) and *cmt1-1* leaves **(F and H)**. Scale bars: 2 μm in **(E)** and **(F)**; 500 nm in **(G)** and **(H)**.

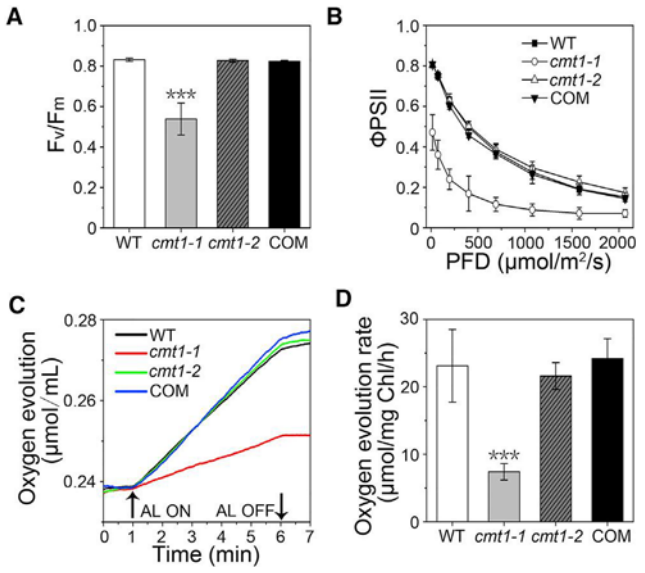

Figure 4. Photosynthetic Activities in WT, *cmt1-1*, *cmt1-2*, and Complemented Plants.

Chlorophyll *a* fluorescence parameters of 3-week-old WT, *cmt1-1*, *cmt1-2*, and COM plants.

(A and B) (A) F_v/F_m: the maximum efficiency of PSII photochemistry; **(B)** ΦPSII: efficiency of PSII electron transport, Data are means ± SD. n = 5 for WT, *cmt1-2*, and COM; n = 10 for *cmt1-1*.

(C) Oxygen evolution rates of WT, *cmt1-1*, *cmt1-2*, and COM plants were measured using isolated thylakoids with potassium ferricyanide as an electron acceptor (chlorophyll content adjusted to 20 μg/ml). AL, actinic light, 500 μmol/m^2/s.

(D) Oxygen evolution rate was calculated from two independent experiments including four replicates. Data are means ± SD. n = 8 for each genotype.

Asterisks indicate statistically significant differences compared with the WT (Mann-Whitney test, ***$P < 0.001$).

Figure 3A) (Demaegd et al., 2014). Members in this family, such as human TMEM165, yeast Gdt1p, and *Arabidopsis* PAM71/CCHA1, have been shown to play a role in calcium or manganese homeostasis (Demaegd et al., 2013; Potelle et al., 2016; Schneider et al., 2016; Wang et al., 2016). CMT1 possesses two conserved E-Φ-G-D-(KR)-(TS) consensus motifs and five putative transmembrane domains, with a central hydrophilic loop between TM3 and TM4. The central loop is rich in acidic residues and might be involved in binding divalent cations (Supplemental Figure 3B and 3C) (Demaegd et al., 2014). Hence, it is reasonable to propose that CMT1 participates in cation homeostasis in chloroplasts. To test this possibility, we measured the total leaf content and chloroplast content of various metals in the wild-type and *cmt1-1* plants using inductively coupled plasma-mass spectrometry (ICP–MS). The total leaf contents of Fe and Cu were higher in *cmt1-1* than in the wild-type, whereas no significant differences were detected for other elements (Mn, Ca, Mg, and Zn) (Figure 6A and Supplemental Table 3). In isolated intact chloroplasts, contents of Mn and Mg were significantly lower in *cmt1-1* than in the wild-type, with the levels of Ca, Fe, Cu, and Zn unchanged (Figure 6B and Supplemental Table 3). Noticeably, even though total leaf contents of Mn and Mg were comparable between wild-type and *cmt1-1* leaf tissue, they showed a significant reduction in the chloroplasts of *cmt1-1* compared with that of wild-type (Figure 6B and Supplemental Table 3). These results indicate that CMT1 affects Mn and Mg homeostasis in the chloroplast.

Reduced levels of Mn and Mg in the *cmt1-1* mutant suggested that CMT1 may be involved in the accumulation of these two cations, which are both required for chloroplast development and function. It is also possible that a change in one of the cations is the primary cause of the developmental defect, which in turn results in a change in the other cation as a secondary effect. To test which ion was the leading cause of the *cmt1-1* phenotype, we attempted to rescue the mutants by supplementing Mn^{2+}, Mg^{2+}, or other cations in the medium as described in Schneider et al. (2016). Although the growth phenotype of *cmt1-1* was not rescued by additional Mn^{2+} or other divalent cations (Supplemental Figure 5A–5D), the F_v/F_m values in the mutant plants were partially restored to 73% of wild-type when grown on medium supplemented with 1 mM Mn^{2+}, and to 83% of wild-type when supplemented with 1.5 mM Mn^{2+}, in contrast to only 60% of the wild-type level in the *cmt1-1* (Figure 6C). However,

Please cite this article in press as: Zhang et al., Inner Envelope CHLOROPLAST MANGANESE TRANSPORTER 1 Supports Manganese Homeostasis and Phototrophic Growth in *Arabidopsis*, Molecular Plant (2018), https://doi.org/10.1016/j.molp.2018.04.007

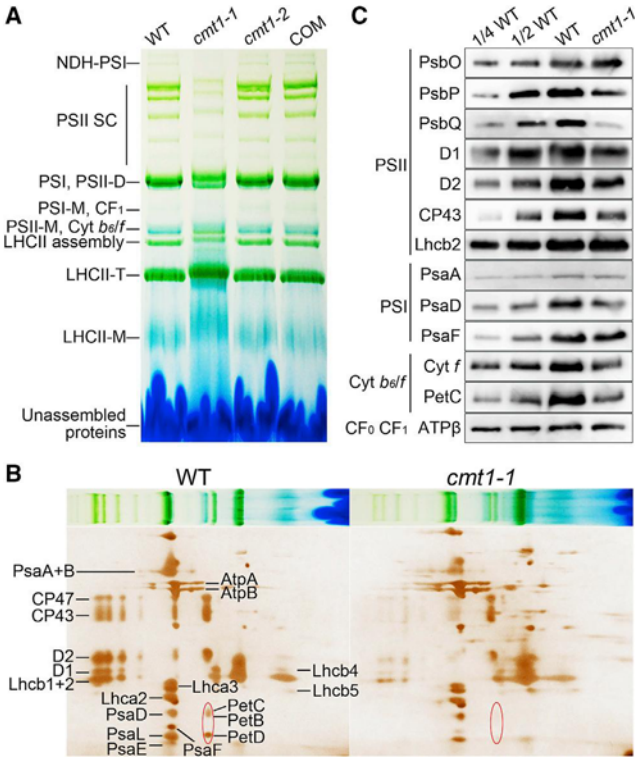

Figure 5. Disruption of CMT1 Causes Altered Accumulation of the Thylakoid Membrane Protein Complexes.

(A) Blue native gel analysis of thylakoid membrane complexes of WT, *cmt1-1*, *cmt1-2*, and COM plants. Thylakoid membranes (equivalent to 10 μg of chlorophyll) were solubilized with 1% (w/v) β-dodecyl-maltoside. NDH-PSI, NDH-PSI super complexes; PSII SC, PSII super complexes; PSII-D, PSII dimer; PSI-M, PSI monomer; CF1, CF_0–CF_1 complex; Cyt b_6/*f*, cytochrome b_6/*f* complexes; LHCII assembly, PSII light-harvesting complex; LHCII-T, PSII light-harvesting complex trimer; LHCII-M, PSII light-harvesting complex monomer.

(B) Thylakoid proteins separated by BN gel in **(A)** (WT and *cmt1-1*) were further subjected to SDS–PAGE and silver stained. Protein identification was based on Fu et al. (2007) and Hou et al. (2015). The red oval circle indicates the location of PetC, B, and D protein.

(C) SDS–PAGE immunoblotting analysis of thylakoid proteins (1 μg of chlorophyll) from WT and *cmt1-1*. Antibodies were applied as indicated.

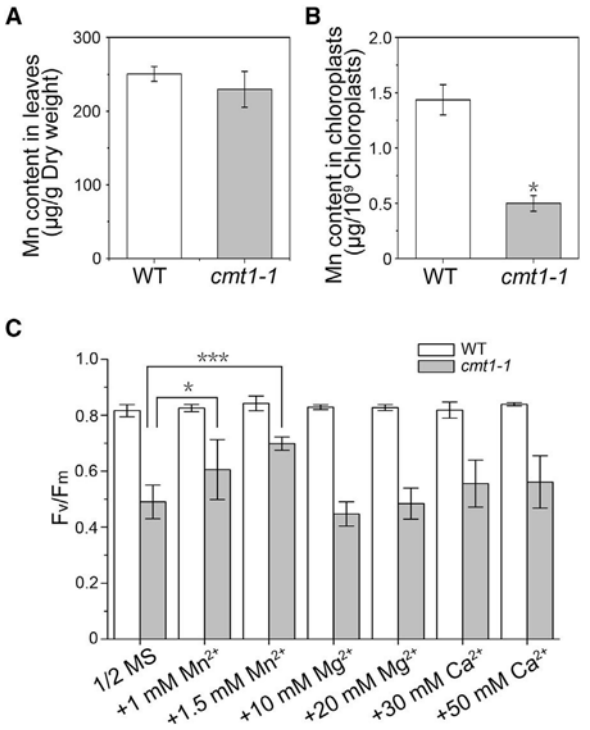

Figure 6. Reduced Mn Content in the *cmt1-1* Chloroplast and Partially Restored Photosynthetic Activity of *cmt1-1* Mutant by Mn^{2+}.

(A and B) Mn contents of leaves **(A)** and intact chloroplasts **(B)** in 3-week-old WT and *cmt1-1* plants. Data are means ± SD. n = 4 for leaf assays, n = 5 for WT, and n = 3 for *cmt1-1* in chloroplast assays.

(C) F_v/F_m value of 3-week-old WT and *cmt1-1* grown on half-strength MS medium supplemented with Mn^{2+}, Mg^{2+}, or Ca^{2+}. Data are means ± SD. n = 4 for WT and n = 8 for *cmt1-1*.

Asterisks indicate statistically significant differences compared with the WT in **(B)** or the control conditions (1/2 MS) in **(C)** (Mann-Whitney test, $^*P < 0.05$, $^{***}P < 0.001$).

the F_v/F_m value of *cmt1-1* was not significantly changed on the medium supplemented with a high concentration of Mg^{2+} or Ca^{2+} (Figure 6C). This result suggested that the photosynthetic defects in the *cmt1-1* mutant may result from Mn deficiency in the chloroplast.

The CMT1 protein is localized in the inner envelope and appears to function in Mn accumulation into the chloroplast. To examine Mn^{2+} transport activity of CMT1, we cloned *CMT1* into the yeast expression vector pYES2 and then introduced it into the *Δsmf1* yeast strain lacking plasma membrane Mn^{2+} transporter SMF1. The *Δsmf1* strain is defective in Mn^{2+} uptake and fails to grow under Mn^{2+}-limited conditions induced by Mn^{2+}-chelator EGTA (Supek et al., 1996). In our experiments, the control (*Δsmf1* transformed with empty pYES2 vector) did not grow on medium containing 10 mM EGTA. The growth defect was restored when the medium was supplemented with 10 μM Mn^{2+} but not with Ca^{2+}, indicating that the *Δsmf1* strain is specifically sensitive to Mn^{2+} deficiency, rather than Ca^{2+} deficiency (Figure 7A). As a positive control, *Δsmf1* transformed with IRT1, an iron transporter that also transports Mn^{2+} (Korshunova et al., 1999), grew well on medium containing 20 mM EGTA (Figure 7A). When transformed with construct containing full-length *CMT1*, *Δsmf1* did not grow under Mn^{2+}-limited conditions (Figure 7A).

We suspected that transit peptide of chloroplast proteins might interfere with the localization or activity of a protein when expressed in the yeast strain (Demaegd et al., 2013). To circumvent this potential problem, the truncated version of *CMT1* lacking the predicted transit peptide (first 66 residues at the N terminus) were fused with GFP ($^{\Delta N66}$*CMT1-GFP*) and cloned into pYES2 vector. The *Δsmf1* yeast cells expressing full-length *CMT1-GFP* and $^{\Delta N66}$*CMT1-GFP* constructs were examined under a confocal microscope. The fluorescence signal from CMT1-GFP gave rise to aggregated puncta in the yeast cells, whereas the $^{\Delta N66}$CMT1-GFP signal overlapped with red fluorescent probe FM4-64 that stained the plasma membrane (Supplemental Figure 6). Thus, $^{\Delta N66}$CMT1 that can be targeted to the plasma membrane in the yeast cells was employed in the complementation assay subsequently.

Please cite this article in press as: Zhang et al., Inner Envelope CHLOROPLAST MANGANESE TRANSPORTER 1 Supports Manganese Homeostasis and Phototrophic Growth in *Arabidopsis*, Molecular Plant (2018), https://doi.org/10.1016/j.molp.2018.04.007

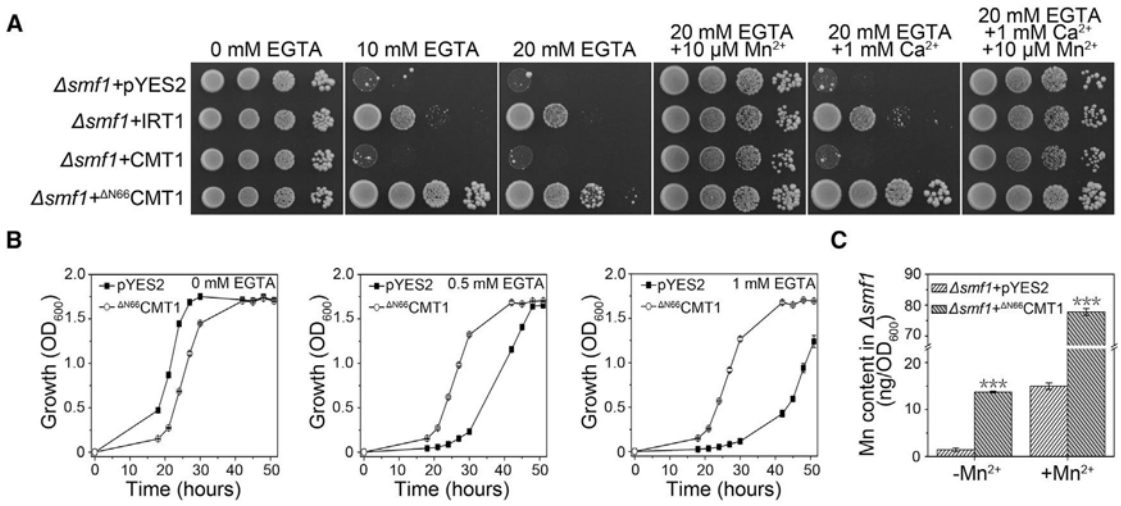

Figure 7. CMT1-Mediated Complementation of Growth Deficiency in *Δsmf1*.

(A) Empty vector (*Δsmf1*+pYES2), *IRT1* (*Δsmf1*+IRT1), *CMT1* (*Δsmf1*+CMT1), and truncated version $^{\Delta N66}$*CMT1* (*Δsmf1*+$^{\Delta N66}$CMT1) were introduced into yeast mutant strain *Δsmf1*. Yeast cells were grown on synthetic medium without uracil (SC-U) containing galactose in the absence or presence of Mn^{2+}-chelator EGTA with the addition of extra Mn^{2+} or Ca^{2+}. The concentrations of EGTA, Mn^{2+}, and Ca^{2+} are indicated on the top. 5 μl (OD_{600} = 0.2) of 10-fold serial dilutions were spotted. Plates were incubated at 30°C for 3–4 days.

(B) Growth curves of yeast cells expressing pYES2 and $^{\Delta N66}$CMT1 were plotted from OD_{600} values. Growth of yeast cells in liquid cultures containing 0, 0.5, or 1 mM EGTA were monitored every 3 h from 18 to 51 h. Data are means ± SD. n = 3.

(C) ICP-MS analysis of Mn content in *Δsmf1* cells expressing pYES2 (*Δsmf1*+pYES2) and $^{\Delta N66}$CMT1 (*Δsmf1*+$^{\Delta N66}$CMT1) cultured in Mn^{2+}-limited or Mn^{2+}-sufficient liquid SC-U medium (OD_{600} = 1.0). Data are means ± SD. n = 3. Asterisks indicate statistically significant differences compared with the negative control (*Δsmf1*+pYES2) (Student's *t*-test, ***$P < 0.001$).

Indeed, the *Δsmf1* containing $^{\Delta N66}$CMT1 construct grew well in the presence of 20 mM EGTA, even better than the strain expressing IRT1 (Figure 7A). Growth curve analysis using liquid culture also consistently indicated that CMT1, without the chloroplast transit peptide, supported the growth of yeast cells under Mn^{2+}-limited conditions (Figure 7B). Moreover, we measured the ionic content in the yeast strains and found that *Δsmf1* expressing $^{\Delta N66}$CMT1 accumulated more Mn than the vector control under both Mn^{2+}-limited and Mn^{2+}-sufficient conditions (Figure 7C), whereas no significant difference was observed with contents of other metal ions (Ca, Mg, Fe, Cu, and Zn) (Supplemental Table 4). Together, these results confirmed that CMT1 mediates Mn^{2+} uptake as a Mn^{2+} transporter.

DISCUSSION

The metal ions, especially Mn, Cu, Fe, and Mg, are crucial components for chloroplast structure and photosynthesis (Pottosin and Shabala, 2016). Transporters that are localized at the inner envelope play a crucial role in ionic fluxes across the chloroplast envelope and thus maintain the homeostasis of metal ions in the photosynthetic organelles. For some metals that function in the thylakoid lumen, transporters in the thylakoid membrane are also required to further deliver the ions from the stroma into the lumen. The best-known mechanism for such transport processes is Cu transport by PAA1 and PAA2. The P-type ATPase PAA1 localized in the inner envelope of chloroplast imports Cu into the stroma, and PAA2 present in the thylakoid membrane delivers Cu further into the lumen where it is incorporated into plastocyanin to participate in photosynthetic electron transport (Shikanai et al., 2003; Abdel-Ghany et al., 2005). An ancient permease PIC1 and a CorA-family transporter in the inner envelope have been shown to function in the delivery of Fe and Mg, respectively, into chloroplasts (Drummond et al., 2006; Duy et al., 2007). The Mn cluster works in the thylakoid lumen side to split water into oxygen, and thus Mn, like Cu, needs to be transported first from the cytosol into the chloroplast and further into the thylakoid lumen. A recent study suggested that PAM71, a UPF0016 family protein localized in the thylakoid membrane, is required for the biogenesis of the Mn cluster possibly by importing Mn into the lumen from the stromal side (Schneider et al., 2016). In the present study, we identified an inner envelope-localized CMT1, a UPF0016 family member highly related to PAM71, that functions as a transporter required for Mn accumulation in the chloroplast. Therefore, we propose that Mn is imported first by CMT1 into the chloroplast stroma and further delivered into the thylakoid lumen by PAM71, supporting the biogenesis of the water-splitting Mn cluster essential for photosynthesis.

Our study provided several lines of evidence to define CMT1 as an inner envelope Mn^{2+} transporter. First, CMT1 protein was predicted to be a chloroplast protein with a typical N-terminal transit peptide for chloroplast import. A proteomic analysis identified CMT1 protein in the inner envelope proteome (Ferro et al., 2003, 2010). We further confirmed that CMT1-GFP fusion is localized to the inner envelope membrane of chloroplasts (Figure 2). Second, ionomic analysis of intact chloroplasts from the wild-type and *cmt1-1* mutant plants by ICP–MS showed that *cmt1-1* chloroplasts displayed a reduced Mn content, indicating that CMT1 plays a key role in Mn^{2+} accumulation in chloroplasts (Figure 6B). Third, the F_v/F_m value in the *cmt1-1* mutant was partially restored when grown on medium supplemented with

Please cite this article in press as: Zhang et al., Inner Envelope CHLOROPLAST MANGANESE TRANSPORTER 1 Supports Manganese Homeostasis and Phototrophic Growth in *Arabidopsis*, Molecular Plant (2018), https://doi.org/10.1016/j.molp.2018.04.007

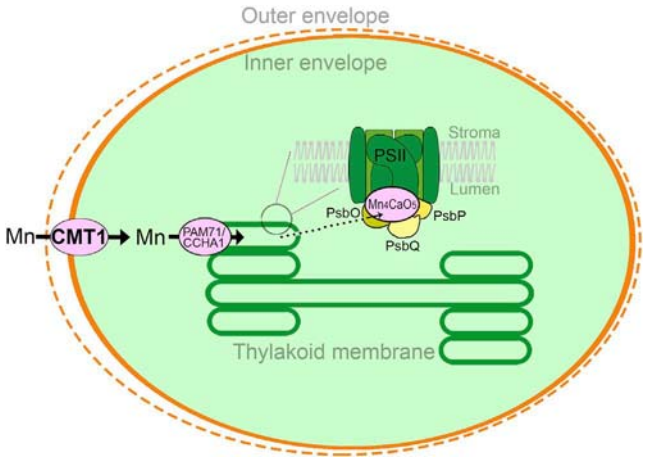

Figure 8. Working Model of Mn Delivery in the Chloroplast.
Mn is transported from the cytosol into the chloroplast stroma through CMT1 localized in the inner envelope and further transferred to the thylakoid lumen by PAM71/CCHA1 in the thylakoid membrane where the Mn cluster is synthesized for oxygen production during photosynthesis.

Mn^{2+} (Figure 6C). Finally, CMT1 complemented the growth deficiency of *Δsmf1*, a yeast strain lacking the Mn uptake transporter SMF1 (Figure 7A). Such complementation was accompanied by a large increase in Mn accumulation in yeast cells under Mn^{2+}-limited conditions (Supplemental Table 4), indicating that CMT1 is capable of mediating the transport of Mn^{2+}. Taken together, these results support our conclusion that CMT1 functions as a Mn^{2+} transporter in the chloroplast inner envelope.

Many of the metal transporters identified so far, including the Mn^{2+} transporters, may be non-selective and transport a broad range of substrates. This makes it difficult to define the physiological substrates of a particular transporter. For instance, as important Mn^{2+} transporters, AtNRAMP1, 3, and 4 also display Fe^{2+} uptake activity in yeast (Thomine et al., 2000; Lanquar et al., 2005; Cailliatte et al., 2010; Castaings et al., 2016). Another Mn^{2+} transporter, AtECA3 is capable of transporting Ca^{2+} and complemented yeast mutant K616, which does not grow in Ca^{2+}-depleted medium (Mills et al., 2008). Therefore, it is possible that CMT1-type Mn transporters, members of the UPF0016 family of proteins, may also transport other metals. In this context, studies on animal and yeast UPF0016 proteins are relevant and present complications in defining substrates of this family of proteins. Human TMEM165 and yeast Gdt1p, which are involved in Mn^{2+} homeostasis of Golgi (Potelle et al., 2016, 2017), also play a vital role in regulating Ca^{2+} and pH balance in Golgi (Demaegd et al., 2013; Colinet et al., 2016). Intriguingly, PAM71, the closest homolog of CMT1 in *Arabidopsis*, is located in the thylakoid membrane and shown to affect Mn^{2+} homeostasis between stroma and thylakoid in one study (Schneider et al., 2016), and to affect Ca^{2+} homeostasis in another study. This protein was also referred to as CCHA1 in an independent study (Wang et al., 2016). In our study, we also collected data that may suggest that CMT1 can mediate Mg transport. For example, CMT1, like the CorA-type Mg transporter MGT10, complemented the growth of Mg^{2+}-uptake deficient *Salmonella typhimurium* strain MM281 under Mg^{2+}-limited conditions (Supplemental Figure 7A), indicating CMT1 might be capable of transporting Mg^{2+}. However, CMT1 did not appear to transport Fe^{2+} or Ca^{2+}, as neither full-length CMT1 nor $^{\Delta N66}$CMT1 could rescue the growth deficiency of *Δfet3/4* (Fe^{2+}-uptake deficient yeast strain) under Fe^{2+}-limited conditions or suppress the sensitivity of *Δgdt1* under high Ca^{2+} conditions (Supplemental Figure 7B and 7C). In ionomic analysis, no significant differences were observed between wild-type and the *cmt1-1* mutant concerning the content of Ca, Fe, Cu, or Zn. Interestingly, a significant decrease in both Mn and Mg levels was found in the *cmt1-1* mutant (Supplemental Table 3). However, supplementing the external medium with Mg^{2+}, unlike addition of Mn^{2+}, failed to improve the growth or F_v/F_m value in the *cmt1-1* mutant (Figure 6C). We thus suspected that the decrease in Mg content in the *cmt1-1* mutant probably resulted from reduced chlorophyll content, representing a secondary effect of defects in chloroplast development and PSII malfunction caused by Mn^{2+} deficiency.

Recent studies suggest that PAM71, NRAMP2, and NRAMP3/4 play critical roles in intracellular Mn distribution and homeostasis that have important consequence on photosynthesis (Lanquar et al., 2010; Schneider et al., 2016; Alejandro et al., 2017). As a result of Mn deficiency in the chloroplast of *cmt1-1* mutant, the Mn cluster in the PSII supercomplex would be defective, leading to a decrease in oxygen-evolving activity (Figure 4). Such a defect would result in a decrease in PSII efficiency and accumulation of reactive oxygen species (Supplemental Figure 8), leading to oxidization of PSII components and other photosynthetic complexes. The immediate targets for such oxidative stress are extrinsic protein PsbO, PsbP and PsbQ, and PSII reaction centers D1 and D2. Indeed, the abundance of all these proteins was severely reduced in the *cmt1-1* mutant plants (Figure 5). Such effects can also be induced by exposing plants to Mn^{2+}-limited conditions as previously reported (Allen et al., 2007; De Bang et al., 2015). From the developmental point of view, upon light exposure, Mn is required for OEC assembly, PSII assembly, and thus thylakoid membrane biogenesis. We envision that increased oxidative stress and defects in thylakoid biogenesis both contribute to the defective chloroplast structure and overall reduction in photosynthesis and stunted growth in the *cmt1-1* mutant. We found that the expression level of *CMT1* was rapidly induced after the etiolated seedlings were exposed to continuous light (Supplemental Figure 9), suggesting that the induced expression of *CMT1* was in accordance with the increasing requirement of Mn. Because Mn requires two steps in transport toward its destination in the thylakoid lumen, both CMT1 in the inner envelope and PAM71/CCHA1 in the thylakoid are essential for Mn delivery and thus for phototrophic growth of the plant. Disruption of either CMT1 or PAM71 should cause similar defects in mutant plants. This hypothesis is supported by the results in this study and studies on PAM71/CCHA1 (Schneider et al., 2016; Wang et al., 2016). Integrating the data in these studies, we proposed a model in which CMT1 functions in Mn^{2+} transport across the inner envelope in chloroplasts, and then Mn^{2+} is further delivered into the lumen by PAM71/CCHA1 (Figure 8).

Please cite this article in press as: Zhang et al., Inner Envelope CHLOROPLAST MANGANESE TRANSPORTER 1 Supports Manganese Homeostasis and Phototrophic Growth in *Arabidopsis*, Molecular Plant (2018), https://doi.org/10.1016/j.molp.2018.04.007

METHODS

Plant Materials and Growth Conditions

Arabidopsis thaliana wild-type (ecotype Columbia-0), the T-DNA insertion line *cmt1-1* (SALK_129037C), and *cmt1-2* (SALK_011783C) were obtained from the Arabidopsis Biological Resource Center. Homozygous individuals were screened by PCR using the primers listed in Supplemental Table 5. The surface-sterilized *Arabidopsis* seeds were planted on half-strength MS containing 1% (w/v) sucrose and 0.8% (w/v) agar (Caisson Labs) (pH 5.8). After stratifying at 4°C for 2 days, the plants were grown in a growth chamber. For soil culture, 10-day-old seedlings after germination on half-strength MS were transferred to the nutrient-rich soil (Pindstrup Mosebrug, Denmark), and then grown in the greenhouse. The conditions in the growth chamber and greenhouse were normal light conditions (90 μmol/m^2/s) with a long-day cycle (16 h light/8 h dark) at 22°C.

RT–PCR and qRT–PCR Analysis

Total RNA was extracted using TRIzol reagent (Invitrogen) according to the manufacturer's instructions. First-strand cDNA was synthesized by M-MLV Reverse Transcriptase (Promega). RT–PCR analysis of gene expression using cDNA of wild-type, *cmt1-1*, *cmt1-2* and complemented plants, included 25 cycles of PCR. qRT–PCR analysis was performed using the FastStart Universal SYBR Green mastermix (Roche) on a CFX Connect Real Time System (Bio-Rad). Target quantifications were performed with specific primer pairs designed using the Primer designing tool in NCBI (https://www.ncbi.nlm.nih.gov/tools/primer-blast/). *ACTIN2* was used as the internal standard in both RT–PCR and qRT–PCR analyses. All primers used are listed in Supplemental Table 5.

Plasmid Constructs and Plant Transformation

For genetic complementation, the full-length genomic DNA of the *CMT1* fragment (a 4552 bp fragment containing a 1975 bp promoter, 2424 bp full-length coding sequence, and 153 bp downstream sequence) was amplified from the genomic DNA of wild-type seedlings and cloned into the binary vector pCAMBIA-1300 via the SphI-BamHI site. To generate the *CMT1* promoter GUS construct (*$CMT1_{pro}$::GUS*), the 1975 bp promoter region upstream of the initial ATG codon was amplified and cloned into the modified pCAMBIA-1300 binary vector with *GUS* reporter gene via the PstI-BamHI site. These constructs were introduced into the *Agrobacterium tumefaciens* GV3101 strain for transformation into *cmt1-1* and wild-type plants by the floral dipping method (Clough and Bent, 1998), respectively. Transgenic plants were screened on half-strength MS medium containing 25 μg/ml hygromycin. The primers used are listed in Supplemental Table 5.

Histochemical GUS Analysis

Histochemical staining for GUS activity was performed as described previously (Sundaresan et al., 1995). Briefly, tissues from the T2 transgenic plants were fixed in 90% ice-cold acetone for 30 min and then washed with staining buffer (0.5 mM $K_4[Fe(CN)_6]$, 0.5 mM $K_3[Fe(CN)_6]$, 0.1% Triton X-100, 10 mM EDTA, and 100 mM sodium phosphate). The samples were incubated in the staining buffer plus 1 mM X-Gluc for 12 h at 37°C. Then the staining buffer was removed, and the samples were destained with 70% ethanol. The expression patterns were recorded with a microscope (SZX16, Olympus).

Subcellular Localization of CMT1

For subcellular localization analysis, the coding sequence (CDS) of *CMT1* was cloned into the pEZS-NL-GFP vector via the EcoRI-BamHI site. The CDS regions of *PAA2* and *RBCS* were amplified and cloned into the pEZS-NL-GFP vector, and the CDS regions of *PIC1* and *OEP7* were amplified and cloned into the pEZS-NL-GFP and pEZS-NL-RFP vectors, respectively, as the suborganellar marker in chloroplast. The primers used are listed in Supplemental Table 5.

Isolation and transient expression in *Arabidopsis* protoplasts was performed as previously described (Yoo et al., 2007). Four-week-old rosette leaves of *Arabidopsis* were cut into slices and digested with Cellulase R-10 and Macerozyme R-10 (Yakult Pharmaceutical). The protoplasts were filtered and washed, then re-suspended in MMG solution. After polyethylene glycol (PEG)-mediated transfection, protoplasts were incubated at 22°C in the dark for 16 h. Images were taken by confocal microscopy (Leica TCS-SL and Lei TCS SP8-MaiTai MP). GFP signals were imaged with excitation at 488 nm, and the emission signal was collected between 493 and 555 nm. The autofluorescence signal of chlorophyll was collected between 650 and 750 nm. The fluorescence signal of RFP was observed with excitation at 561 nm, and the emission signal was collected between 568 and 636 nm. For colocalization analysis, the Colocalization Finder plugin of Image J was used.

Leaf Morphology and Chloroplast Ultrastructure

The 3-week-old rosette leaves were cut into small pieces and fixed in 2.5% glutaraldehyde (prepared in 0.1 M phosphate buffer [pH 7.2]) under mild vacuuming and kept at 4°C overnight. Samples for semithin sections (1 μm) and ultrathin sections (60 nm) were prepared as described previously (Zheng and Wang, 2011). For leaf morphology, cross-sections were stained with a counterstain (containing sarranine and methyl violet) and then photographed under a microscope (SZX16, Olympus). For ultrastructure of chloroplasts, micrographs were taken under a transmission electron microscope (H7650, Hitachi).

Measurement of Starch Content

Rosette leaves were harvested from 3-week-old plants grown on half-strength MS medium. The starch content was measured using the anthrone colorimetry method.

Chlorophyll *a* Fluorescence Measurements

Intact leaves from 3-week-old plants were dark adapted for 30 min before they were measured with a FMS2 fluorometer (Hansatech). The chlorophyll *a* fluorescence parameters F_o, F_m, and F_s were measured and calculated as described (Fu et al., 2007). F_v/F_m was calculated as $(F_m - F_o)/F_m$, and ΦPSII was defined as $(F'_m - F_s)/F'_m$. 1 − qL was equal to $(F'_o/F_s)(F'_m - F_s)/(F'_m - F'_o)$. NPQ was calculated as $(F_m - F'_m)/F'_m$.

Oxygen Evolution Rate

Oxygen evolution was measured as described (Lima et al., 2006). Briefly, leaves were homogenized in ice-cold homogenization buffer (0.33 M sorbitol, 5 mM $MgCl_2$, 10 mM NaCl, 2 mM EDTA, and 30 mM MOPS, pH adjusted to 7.8 with KOH). Crude chloroplasts were filtered through two layers of Miracloth (Calbiochem) and centrifuged at 700 *g* for 5 min. The thylakoid pellets were re-suspended in the homogenization buffer and adjusted to 20 μg chlorophyll/ml. Oxygen evolution was measured at 25°C with an oxygen electrode (Chlorolab2, Hansatech) using 0.5 mM potassium ferricyanide as an electron acceptor.

Immunoblotting Analysis

Thylakoid membrane protein samples corresponding to equal amounts of chlorophyll (1 μg) were separated on 15% SDS–PAGE gels and transferred to PVDF membranes. After blocking nonspecific binding with 5% milk, the blot was subsequently incubated with antibodies generated against the indicated proteins and detected using a SuperSignal West Pico Trial kit (Thermo Scientific).

BN–PAGE and 2D SDS–PAGE

BN–PAGE was performed as described (Asakura et al., 2004; Lima et al., 2006). Thylakoid membrane samples containing equal amounts of chlorophyll (10 μg) were loaded onto a 5%–13.5% native gradient gel. Electrophoresis was performed at 100 V at 4°C (PowerSac Universal, Bio-Rad). The cathode buffer initially contained 0.01% Serva Blue G dye (Serva) and was replaced by cathode buffer free of dye after the blue running front had moved about one-third of the desired total running.

Please cite this article in press as: Zhang et al., Inner Envelope CHLOROPLAST MANGANESE TRANSPORTER 1 Supports Manganese Homeostasis and Phototrophic Growth in *Arabidopsis*, Molecular Plant (2018), https://doi.org/10.1016/j.molp.2018.04.007

For 2D SDS–PAGE analysis, lanes of blue native gel were excised with a razor blade and soaked in 2× SDS sample buffer containing 2.5% β-mercaptoethanol for 10 min at room temperature. Each lane with denatured proteins was placed on top of 1.0-mm-thick 12% SDS–PAGE and electrophoresed at 90 V. After electrophoresis, gels were stained with a protein silver stain kit (CWBIO) and photographed with the Gel Doc XR+ System (Bio-Rad).

Measurement of Metal Content in Leaf and Intact Chloroplasts by ICP–MS

After growing for 3 weeks on half-strength MS medium containing 1% sucrose, the leaves of the wild-type and *cmt1-1* plants were collected for isolating the intact chloroplasts according to the method described previously (Aronsson and Jarvis, 2002; Shang et al., 2010) with slight modifications. During the isolation procedure, the plant material was kept at 4°C. After homogenizing 10 g fresh weight of leaf samples in ice-cold Grind Buffer (0.33 M sorbitol, 10 mM EDTA, 50 mM HEPES, and 0.5 g/l BSA, pH adjusted to 8.0 with KOH), the homogenate was filtered through double layers of Miracloth (Calbiochem) and concentrated by centrifugation for 5 min at 700 *g* at 4°C using a swing-out rotor (Centrifuge 5810R, Eppendorf). The pellets were gently re-suspended in Grind Buffer with a brush and then loaded onto a two-step 40% (v/v)/80% (v/v) Percoll (GE Healthcare) gradient. After centrifugation for 15 min at 2000 *g* at 4°C, the band containing intact chloroplasts was isolated from the interface of the two phases, and then the intact chloroplasts were carefully recovered and washed in SH (0.33 M sorbitol and 50 mM HEPES, pH adjusted to 8.0 with KOH).

Leaves and intact chloroplasts were collected and dried at 70°C for 72 h. The samples were then digested with concentrated HNO_3 (ultrapure) in a digester (DigiBlock ED16, LabTech). Ion concentration was measured by ICP–MS (NexION 300, Perkin-Elmer).

Heterologous Expression of CMT1 in Yeast

For complementation of the yeast mutants, the full-length CDS and a truncated version of *CMT1* (without the first 66 amino acids corresponding to the cTP region) were cloned into the pYES2 vector with a GFP-tag using the EcoRI-XbaI site. As a positive control, the CDS of *IRT1* was cloned into the pYES2 vector using the EcoRI-XbaI site. The pYES2 empty vector and recombinant plasmids were introduced into different yeast (*Saccharomyces cerevisiae*) mutant strains as described in the Yeast Protocols Handbook (Clontech Laboratories). The yeast strains used in this study were the Mn^{2+}-uptake deficient mutant *Δsmf1* (*MATa his2Δ0 met15Δ0 ura3Δ0 YOL122c::KanMX4*), the Fe^{2+}-uptake deficient double-mutant *Δfet3/4* (*MATa ade6 can1 his3 leu2 trp1 ura3 fet3-2::HIS3 fet4-LEU*), and high Ca^{2+} sensitive mutant *Δgdt1* (*MATa his3Δ1 leu2Δ0 met15Δ0 ura3Δ0 gdt1::kanMX4*). The cells transformed with the indicated constructs were grown on synthetic medium containing amino acids without uracil (SC-U). Complementation of the *Δsmf1* phenotype was tested on a synthetic medium containing 0.67% yeast nitrogen base, 2% galactose, 0.2% appropriate amino acids (omitted uracil), and 2% agar; pH was buffered at 6.0 with 50 mM MES and supplemented with 0, 10, or 20 mM EGTA. Complementation of the *Δfet3/4* phenotype was tested on synthetic medium containing 0.67% yeast nitrogen base, 2% galactose, 0.2% appropriate amino acids (omitted uracil), and 2% agar; pH was buffered at 5.5 with 50 mM MES in the presence of 0, 50, or 100 μM BPDS. The high Ca^{2+} sensitivity of *Δgdt1* was tested on synthetic medium containing 0.67% yeast nitrogen base, 2% galactose, 0.2% appropriate amino acids (omitted uracil), and 2% agar; pH was buffered at 6.0 in the presence of 0, 300, or 400 mM Ca^{2+}. Yeast cells were harvested by centrifugation at 700 *g* for 5 min and washed twice with sterile water. The cells were re-suspended and adjusted to OD_{600} = 0.2; 5 μl of 10-fold serial dilutions were spotted onto the plates as indicated above. The plates were incubated at 30°C for 3–5 days before being photographed.

The yeast cells with different vectors were pre-cultured overnight to OD_{600} = 1.0, harvested by centrifugation at 700 *g* for 5 min, and washed twice with sterile water. The samples were dried at 70°C for 72 h and then digested with concentrated HNO_3 (ultrapure) in a digester (DigiBlock ED16, LabTech). Ion concentration was measured by ICP–MS (NexION 300, Perkin-Elmer).

Complementation of *Salmonella typhimurium* Mutant Strain MM281

For complementation of the *Salmonella typhimurium* mutants, CDS of *CMT1* was amplified and cloned into pTrc99A vector by the EcoRI-BamHI site. The constructs were transformed into MM281 cells by electroporation (Gene pulser Xcell, Bio-Rad). Cells were plated on LB medium supplemented with 10 mM Mg^{2+} and appropriate antibiotics (50 μg/ml ampicillin and 34 μg/ml chloramphenicol) and incubated at 37°C overnight. After verification by PCR, the MM281 transformed with the indicated constructs were prepared for Mg^{2+} uptake assay. The MM281 cells containing different constructs were cultured in liquid LB medium with the same antibiotics to OD_{600} = 0.6. IPTG (50 μM) was added to induce the expression of CMT1. The cells were adjusted to OD_{600} = 1.0; 2 μl of 10-fold serial dilutions were spotted onto N-minimal medium (Mao et al., 2014) supplemented with different concentrations of $MgSO_4$ (10 μM, 100 μM, 500 μM, 1 mM, 10 mM, and 100 mM). The plates were incubated at 37°C for 2 days before being photographed.

ACCESSION NUMBERS

Sequence data from this article can be found in the *Arabidopsis* Information Resource (TAIR) database under the following accession number: TAIR: *CMT1* (AT4G13590).

SUPPLEMENTAL INFORMATION

Supplemental Information is available at *Molecular Plant Online*.

FUNDING

This work was supported by the National Natural Science Foundation of China (31770267 and 31670236) and the National Science Foundation (MCB-1715764).

AUTHOR CONTRIBUTIONS

B.Z., C.Z., W.L., and S.L. designed the research. B.Z., C.Z., C.L., Y.J., and L.J. carried out the experiments. B.Z., C.Z., Y.W., L.Y., A.F., W.L., and S.L. analyzed the data. L.Y., A.F., J.S., and F.Z. provided technical assistance. B.Z., C.Z., W.L., and S.L. wrote the manuscript.

ACKNOWLEDGMENTS

We thank Dr. Chaofeng Huang and Linghuo Jiang for the yeast mutant strains used in this work, Dr. Fangjie Zhao for advice on ICP–MS analysis, Dr. Yufen Che, Pingyong Xu, and Dandan Mao for experimental support, and Jiangsu Collaborative Innovation Center for Modern Crop Production for technical support. No conflict of interest declared.

Received: November 29, 2017
Revised: April 19, 2018
Accepted: April 23, 2018
Published: May 4, 2018

REFERENCES

Abdel-Ghany, S.E., Muller-Moule, P., Niyogi, K.K., Pilon, M., and Shikanai, T. (2005). Two P-type ATPases are required for copper delivery in *Arabidopsis thaliana* chloroplasts. Plant Cell **17**:1233–1251.

Alejandro, S., Cailliatte, R., Alcon, C., Dirick, L., Domergue, F., Correia, D., Castaings, L., Briat, J.F., Mari, S., and Curie, C. (2017). Intracellular distribution of manganese by the trans-Golgi network transporter NRAMP2 is critical for photosynthesis and cellular redox homeostasis. Plant Cell **29**:3068–3084.

Please cite this article in press as: Zhang et al., Inner Envelope CHLOROPLAST MANGANESE TRANSPORTER 1 Supports Manganese Homeostasis and Phototrophic Growth in *Arabidopsis*, Molecular Plant (2018), https://doi.org/10.1016/j.molp.2018.04.007

Allen, M.D., Kropat, J., Tottey, S., Del Campo, J.A., and Merchant, S.S. (2007). Manganese deficiency in *Chlamydomonas* results in loss of photosystem II and MnSOD function, sensitivity to peroxides, and secondary phosphorus and iron deficiency. Plant Physiol. **143**: 263–277.

Aronsson, H., and Jarvis, P. (2002). A simple method for isolating import-competent *Arabidopsis* chloroplasts. FEBS Lett. **529**:215–220.

Asakura, Y., Hirohashi, T., Kikuchi, S., Belcher, S., Osborne, E., Yano, S., Terashima, I., Barkan, A., and Nakai, M. (2004). Maize mutants lacking chloroplast FtsY exhibit pleiotropic defects in the biogenesis of thylakoid membranes. Plant Cell **16**:201–214.

Cailliatte, R., Schikora, A., Briat, J.-F., Mari, S., and Curie, C. (2010). High-affinity manganese uptake by the metal transporter NRAMP1 is essential for *Arabidopsis* growth in low manganese conditions. Plant Cell **22**:904–917.

Carraretto, L., Teardo, E., Checchetto, V., Finazzi, G., Uozumi, N., and Szabo, I. (2016). Ion channels in plant bioenergetic organelles, chloroplasts and mitochondria: from molecular identification to function. Mol. Plant **9**:371–395.

Castaings, L., Caquot, A., Loubet, S., and Curie, C. (2016). The high-affinity metal transporters NRAMP1 and IRT1 team up to take up iron under sufficient metal provision. Sci. Rep. **6**:37222.

Che, Y., Fu, A., Hou, X., McDonald, K., Buchanan, B.B., Huang, W., and Luan, S. (2013). C-terminal processing of reaction center protein D1 is essential for the function and assembly of photosystem II in *Arabidopsis*. Proc. Natl. Acad. Sci. USA **110**:16247–16252.

Clough, S.J., and Bent, A.F. (1998). Floral dip: a simplified method for *Agrobacterium*-mediated transformation of *Arabidopsis thaliana*. Plant J. **16**:735–743.

Colinet, A.-S., Sengottaiyan, P., Deschamps, A., Colsoul, M.-L., Thines, L., Demaegd, D., Duchêne, M.-C., Foulquier, F., Hols, P., and Morsomme, P. (2016). Yeast Gdt1 is a Golgi-localized calcium transporter required for stress-induced calcium signaling and protein glycosylation. Sci. Rep. **6**:24282.

De Bang, T.C., Petersen, J., Pedas, P.R., Rogowska-Wrzesinska, A., Jensen, O.N., Schjoerring, J.K., Jensen, P.E., Thelen, J.J., and Husted, S. (2015). A laser ablation ICP-MS based method for multiplexed immunoblot analysis: applications to manganese-dependent protein dynamics of photosystem II in barley (*Hordeum vulgare* L.). Plant J. **83**:555–565.

Demaegd, D., Colinet, A.-S., Deschamps, A., and Morsomme, P. (2014). Molecular evolution of a novel family of putative calcium transporters. PLoS One **9**:e100851.

Demaegd, D., Foulquier, F., Colinet, A.-S., Gremillon, L., Legrand, D., Mariot, P., Peiter, E., Van Schaftingen, E., Matthijs, G., and Morsomme, P. (2013). Newly characterized Golgi-localized family of proteins is involved in calcium and pH homeostasis in yeast and human cells. Proc. Natl. Acad. Sci. USA **110**:6859–6864.

Drummond, R.S.M., Tutone, A., Li, Y.C., and Gardner, R.C. (2006). A putative magnesium transporter AtMRS2-11 is localized to the plant chloroplast envelope membrane system. Plant Sci. **170**:78–89.

Duy, D., Wanner, G., Meda, A.R., von Wiren, N., Soll, J., and Philippar, K. (2007). PIC1, an ancient permease in *Arabidopsis* chloroplasts, mediates iron transport. Plant Cell **19**:986–1006.

Ferreira, K.N., Iverson, T.M., Maghlaoui, K., Barber, J., and Iwata, S. (2004). Architecture of the photosynthetic oxygen-evolving center. Science **303**:1831–1838.

Ferro, M., Brugière, S., Salvi, D., Seigneurin-Berny, D., Court, M., Moyet, L., Ramus, C., Miras, S., Mellal, M., Le Gall, S., et al. (2010). AT_CHLORO, a comprehensive chloroplast proteome database with subplastidial localization and curated information on envelope proteins. Mol. Cell. Proteomics **9**:1063–1084.

Ferro, M., Salvi, D., Brugière, S., Miras, S., Kowalski, S., Louwagie, M., Garin, J., Joyard, J., and Rolland, N. (2003). Proteomics of the chloroplast envelope membranes from *Arabidopsis thaliana*. Mol. Cell. Proteomics **2**:325–345.

Finazzi, G., Petroutsos, D., Tomizioli, M., Flori, S., Sautron, E., Villanova, V., Rolland, N., and Seigneurin-Berny, D. (2014). Ions channels/transporters and chloroplast regulation. Cell Calcium **58**:86–97.

Fu, A., He, Z., Cho, H.S., Lima, A., Buchanan, B.B., and Luan, S. (2007). A chloroplast cyclophilin functions in the assembly and maintenance of photosystem II in *Arabidopsis thaliana*. Proc. Natl. Acad. Sci. USA **104**:15947–15952.

Hou, X., Fu, A., Garcia, V.J., Buchanan, B.B., and Luan, S. (2015). PSB27: a thylakoid protein enabling *Arabidopsis* to adapt to changing light intensity. Proc. Natl. Acad. Sci. USA **112**:1613–1618.

Korshunova, Y.O., Eide, D., Clark, W.G., Guerinot, M.L., and Pakrasi, H.B. (1999). The IRT1 protein from *Arabidopsis thaliana* is a metal transporter with a broad substrate range. Plant Mol. Biol. **40**:37–44.

Lanquar, V., Lelièvre, F., Bolte, S., Hamès, C., Alcon, C., Neumann, D., Vansuyt, G., Curie, C., Schröder, A., Krämer, U., et al. (2005). Mobilization of vacuolar iron by AtNRAMP3 and AtNRAMP4 is essential for seed germination on low iron. EMBO J. **24**:4041–4051.

Lanquar, V., Ramos, M.S., Lelievre, F., Barbier-Brygoo, H., Krieger-Liszkay, A., Kramer, U., and Thomine, S. (2010). Export of vacuolar manganese by AtNRAMP3 and AtNRAMP4 is required for optimal photosynthesis and growth under manganese deficiency. Plant Physiol. **152**:1986–1999.

Lee, Y.J., Kim, D.H., Kim, Y.W., and Hwang, I. (2001). Identification of a signal that distinguishes between the chloroplast outer envelope membrane and the endomembrane system *in vivo*. Plant Cell **13**:2175–2190.

Lee, D.W., Lee, S., Lee, G.-J., Lee, K.H., Kim, S., Cheong, G.-W., and Hwang, I. (2006). Functional characterization of sequence motifs in the transit peptide of *Arabidopsis* small subunit of rubisco. Plant Physiol. **140**:466–483.

Lima, A., Lima, S., Wong, J.H., Phillips, R.S., Buchanan, B.B., and Luan, S. (2006). A redox-active FKBP-type immunophilin functions in accumulation of the photosystem II supercomplex in *Arabidopsis thaliana*. Proc. Natl. Acad. Sci. USA **103**:12631–12636.

Mao, D., Chen, J., Tian, L., Liu, Z., Yang, L., Tang, R., Li, J., Lu, C., Yang, Y., Shi, J., et al. (2014). *Arabidopsis* transporter MGT6 mediates magnesium uptake and is required for growth under magnesium limitation. Plant Cell **26**:2234–2248.

Mills, R.F., Doherty, M.L., Lopez-Marques, R.L., Weimar, T., Dupree, P., Palmgren, M.G., Pittman, J.K., and Williams, L.E. (2008). ECA3, a Golgi-localized P2A-type ATPase, plays a crucial role in manganese nutrition in *Arabidopsis*. Plant Physiol. **146**:116–128.

Nelson, N., and Yocum, C.F. (2006). Structure and function of photosystems I and II. Annu. Rev. Plant Biol. **57**:521–565.

Nouet, C., Motte, P., and Hanikenne, M. (2011). Chloroplastic and mitochondrial metal homeostasis. Trends Plant Sci. **16**:395–404.

Oh, Y.J., and Hwang, I. (2015). Targeting and biogenesis of transporters and channels in chloroplast envelope membranes: unsolved questions. Cell Calcium **58**:122–130.

Potelle, S., Dulary, E., Climer, L., Duvet, S., Morelle, W., Vicogne, D., Lebredonchel, E., Houdou, M., Spriet, C., Krzewinski-Recchi, M.A., et al. (2017). Manganese-induced turnover of TMEM165. Biochem. J. **474**:1481–1493.

Potelle, S., Morelle, W., Dulary, E., Duvet, S., Vicogne, D., Spriet, C., Krzewinski-Recchi, M.A., Morsomme, P., Jaeken, J., Matthijs, G., et al. (2016). Glycosylation abnormalities in Gdt1p/TMEM165

Please cite this article in press as: Zhang et al., Inner Envelope CHLOROPLAST MANGANESE TRANSPORTER 1 Supports Manganese Homeostasis and Phototrophic Growth in *Arabidopsis*, Molecular Plant (2018), https://doi.org/10.1016/j.molp.2018.04.007

deficient cells result from a defect in Golgi manganese homeostasis. Hum. Mol. Genet. **25**:1489–1500.

Pottosin, I., and Shabala, S. (2016). Transport across chloroplast membranes: optimizing photosynthesis for adverse environmental conditions. Mol. Plant **9**:356–370.

Roose, J.L., and Pakrasi, H.B. (2004). Evidence that D1 processing is required for manganese binding and extrinsic protein assembly into photosystem II. J. Biol. Chem. **279**:45417–45422.

Schneider, A., Steinberger, I., Herdean, A., Gandini, C., Eisenhut, M., Kurz, S., Morper, A., Hoecker, N., Ruhle, T., Labs, M., et al. (2016). The evolutionarily conserved protein PHOTOSYNTHESIS AFFECTED MUTANT71 is required for efficient manganese uptake at the thylakoid membrane in *Arabidopsis*. Plant Cell **28**:892–910.

Shang, Y., Yan, L., Liu, Z.Q., Cao, Z., Mei, C., Xin, Q., Wu, F.Q., Wang, X.F., Du, S.Y., Jiang, T., et al. (2010). The Mg-chelatase H subunit of *Arabidopsis* antagonizes a group of WRKY transcription repressors to relieve ABA-responsive genes of inhibition. Plant Cell **22**:1909–1935.

Shen, J.R. (2015). The structure of photosystem II and the mechanism of water oxidation in photosynthesis. Annu. Rev. Plant Biol. **66**:23–48.

Shikanai, T., Müller-Moulé, P., Munekage, Y., Niyogi, K.K., and Pilon, M. (2003). PAA1, a P-type ATPase of *Arabidopsis*, functions in copper transport in chloroplasts. Plant Cell **15**:1333–1346.

Sundaresan, V., Springer, P., Volpe, T., Haward, S., Jones, J.D., Dean, C., Ma, H., and Martienssen, R. (1995). Patterns of gene action in plant development revealed by enhancer trap and gene trap transposable elements. Genes Dev. **9**:1797–1810.

Supek, F., Supekova, L., Nelson, H., and Nelson, N. (1996). A yeast manganese transporter related to the macrophage protein involved in conferring resistance to mycobacteria. Proc. Natl. Acad. Sci. USA **93**:5105–5110.

Theg, S.M., and Wollman, F.A. (2014). Plastid Biology (New York: Springer).

Thomine, S., Wang, R., Ward, J.M., Crawford, N.M., and Schroeder, J.I. (2000). Cadmium and iron transport by members of a plant metal transporter family in *Arabidopsis* with homology to *Nramp* genes. Proc. Natl. Acad. Sci. USA **97**:4991–4996.

Wang, C., Xu, W., Jin, H., Zhang, T., Lai, J., Zhou, X., Zhang, S., Liu, S., Duan, X., Wang, H., et al. (2016). A putative chloroplast-localized Ca^{2+}/H^{+} antiporter CCHA1 is involved in calcium and pH homeostasis and required for PSII function in *Arabidopsis*. Mol. Plant **9**:1183–1196.

Yoo, S.D., Cho, Y.H., and Sheen, J. (2007). *Arabidopsis* mesophyll protoplasts: a versatile cell system for transient gene expression analysis. Nat. Protoc. **2**:1565–1572.

Zheng, Y., and Wang, Z. (2011). Contrast observation and investigation of wheat endosperm transfer cells and nucellar projection transfer cells. Plant Cell Rep. **30**:1281–1288.